

Cite this: *Chem. Sci.*, 2023, 14, 10249

All publication charges for this article have been paid for by the Royal Society of Chemistry

Received 7th August 2023
Accepted 5th September 2023DOI: 10.1039/d3sc04128j
rsc.li/chemical-science

Introduction

The design of efficient orthogonal reactions for highly chemo- and regioselective bioconjugations is a major scientific challenge.^{1–3} Dynamic covalent chemistry (DCC), allowing for adaptation through component exchange and selection in response to chemical/physical/environmental agents under equilibrium/out-of-equilibrium conditions,^{4,5} may provide an efficient approach towards this goal.^{6–8} In particular, the widely applicable Schiff base formation reactions represent a promising procedure for the modification of biomolecules.⁹ Whilst the reaction of oximes and hydrazides with naturally occurring aldehydes has been significantly exploited,^{10,11} only a handful of biologically relevant examples relying on aldimine formation have been described.^{12–15} This is a direct consequence of the high tendency of imines to be hydrolyzed in the presence of water, a particularly challenging feature to be overcome (Fig. 1a).^{16,17} Still, the ability of pyridoxal phosphate (PLP) dependent enzymes to form imine bonds *in vivo* infers that a correct design of reactive aldehydes may provide a pathway for performing this reversible chemistry under physiological conditions.^{18,19}

Supramolecular multivalency effects enhance imine formation in aqueous medium allowing for dynamic modification of enzymatic activity†

Ferran Esteve, * Fidan Rahmatova and Jean-Marie Lehn *

Imine formation under physiological conditions represents a challenging reaction due to the strong propensity of aldimines to be hydrolyzed. Herein we disclose the remarkable effect of supramolecular multivalency on increasing imine stability. A family of reactive aldehydes was synthesized bearing supramolecularly-active sites within their structure. The imine formation activity for such aldehydes was evaluated and compared with model aldehydes. The reaction of the best-performing species – containing two carboxylate groups with a set of amines showed a significant decrease in imine yields as the degree of supramolecular multivalency between sidechains decreased. The reversible conjugation of amino acid derivatives and small peptides was also assayed, with excellent selectivities for the imine formation at the $\text{N}\alpha$ position even in substrates containing competing sites. Preliminary results on protein bioconjugation revealed that a model enzyme could be dynamically inhibited upon reaction with the aldehyde, with its native activity being recovered by displacing the imine bonds with a suitable chemical effector (*i.e.*, acylhydrazide).

Significant progress has been made in the last decade towards efficient aldimine formation in water. For instance, hydrophobic effects have offered many advantages as the lipophilic groups surrounding the imine motifs shield to some extent such reversible bonds from being hydrolyzed.^{20–22} This approach has been further exploited by performing imine

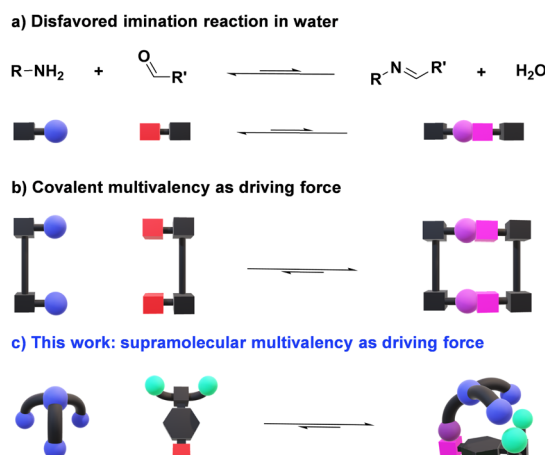


Fig. 1 Schematic representations of imine formation in aqueous medium: (a) imination intrinsically disfavored by hydrolysis; (b) increase in imine formation by covalent multivalency; (c) proposed secondary supramolecular interactions as driving force for enhancing condensation reactions in water. Color code: red boxes for aldehyde CHO; blue spheres for amino groups; light green spheres for negatively charged units; purple sphere + pink box for imine bonds.

Laboratoire de Chimie Supramoléculaire, Institut de Science et d'Ingénierie Supramoléculaires (ISIS), Université de Strasbourg, 8 allée Gaspard Monge, 67000 Strasbourg, France. E-mail: estevefranch@unistra.fr; lehn@unistra.fr

† Electronic supplementary information (ESI) available: Experimental section, main text support figures and schemes, copies of ^1H , ^{13}C NMR, and HRMS spectra, MALDI analyses, DFT cartesian coordinates. See DOI: <https://doi.org/10.1039/d3sc04128j>

condensations in confined apolar arrangements, in which the hydrophobic environments generated within molecular microreactors (*e.g.*, micelles and molecular containers) led to remarkable results.^{23–25} The synthesis of complex 3D-architectures has also been achieved by exploiting multivalency.^{26–28} In these cases, the simultaneous cleavage of multiple dynamic covalent bonds – clearly more challenging than breaking a single bond – further decreases the tendency of imines to hydrolyze in aqueous medium (Fig. 1b).²⁹ Despite the promising advances reached, most of the reported systems are only stable at basic pH or in the presence of certain thermodynamic templates, hampering the use of such designs for dynamic biological applications.^{30,31} The most common approach for overcoming these limitations relies on the coupling of fast and site-selective reversible imination steps with irreversible post-modification reactions (*e.g.*, imine reduction), at expense of the dynamic nature of the systems.^{32–36}

Considering these precedents, we surmised that the presence of secondary supramolecular forces between the aldehyde and amine sidechains could result in high-yielding condensation reactions (Fig. 1c), even in competitive media. This is indeed a driving force in PLP-mediated biological transformations, with the related aldimine intermediates being stabilized through networks of supramolecular interactions with different units elegantly preorganized in active pockets of enzymes.³⁷ Related cooperative non-covalent forces between the two components of the dynamic adduct are here described as supramolecular multivalent effects.

Rationale

Some key factors must be considered when discussing imination reactions in water. Firstly, imines will only be effectively generated in aqueous solutions when the optimal balance between aldehyde reactivity and solubility is met. Further, aldimine products should not precipitate in the medium, as this would act as a kinetic trap, precluding a satisfactory evaluation of the thermodynamic features of the systems.³⁸ One may however remark, that in certain instances, precipitation of the condensate may select for the desired derivative. In addition, hydration of the aldehyde partner competes with imine formation, albeit the same structural factors favoring hydration could also be advantageous for the generation of the imine. It must be noted, however, that whereas the nucleophilic addition of a primary amine would be expected to correlate well with hydration, the subsequent water elimination step may show an opposite trend.¹⁷ Bearing these considerations in mind, we designed a novel family of aldehydes, namely A7, A8, and A9 (Scheme S1†) derived from the quite reactive precursor 2,3,4,5,6-pentafluorobenzaldehyde (A6) to study the role of supramolecular interactions in accomplishing high imine yields under physiological conditions.³⁹ One may predict that such supramolecular multivalency might be strong enough to enhance the thermodynamic stability of imines over hydrolysis (Fig. 1c).^{40,41}

Results and discussion

Evaluation of imine formation activity and of attractive supramolecular forces

To evaluate the relative efficiency of imine formation, the aldehydes A0–A5 were selected and their activity was investigated in comparison to the results obtained for A6–9. A few earlier studies have shown that aldehydes derived from pyridine (A1, Fig. 2) or aldehydes that contain strongly electron-withdrawing units in *ortho*-position to the carbonyl group (A3, Fig. 2) can lead to high activities towards the formation of imines in aqueous media.^{14,39,42,43} Two pyridoxal-derided species, namely A4 and A5, were also considered as such compounds are known to yield highly efficient Schiff base formation. The tris-amine TREN (T) was selected as model amine to test multivalency since the presence of additional positively charged moieties in the structure, +2 or +3 depending on the pH,⁴⁴ serves as an optimal scenario for assaying the role of secondary electrostatic interactions between the pendant arms of the two components of the imine (*i.e.*, aldehyde and amine). Besides, its chemical properties can showcase the reactivity differences between the terminal-amino group and Nε-sites of Lys residues present in proteins.^{45,46}

Condensation reactions were followed by the appearance of the imine CH signal in the ¹H-NMR spectra shifted to lower δ with respect to the peak of the parent aldehyde. The relative abundance of imine and hydrate were determined by the integration of aldehyde and imine/hydrate peaks.¹⁷ The two reagents were mixed in a 1:1 molar ratio using a phosphate

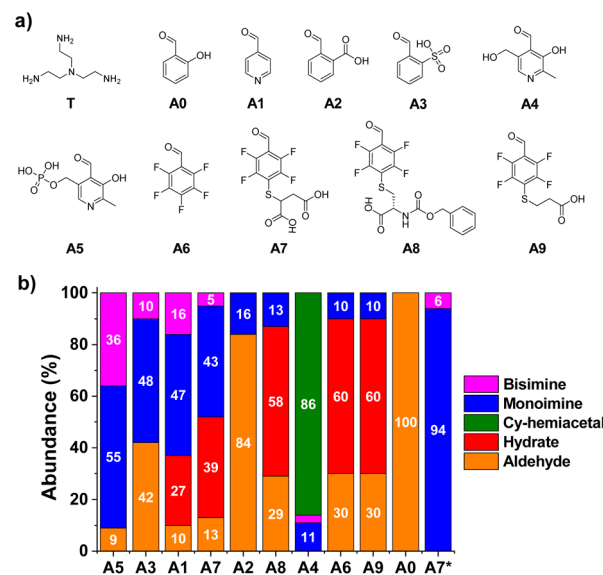


Fig. 2 (a) Chemical structures and (b) component abundance (%) as calculated from ¹H NMR spectra (500 MHz, 295 K, D₂O) for the tested aldehydes upon reaction with T. Reaction conditions: D₂O (pD = 7.2, phosphate buffer 50 mM), 295 K, 1 h, [AX] = [T] = 5 mM. A7*: [A7] = 5 mM, [T] = 50 mM. Cy-hemiacetal: cyclic hemiacetal after intramolecular ring-closing condensation of A4. Aldehydes sorted with decreasing values of monoamine abundances. The abundances of the bisimines were calculated considering the integration of two equivalent CHO protons.



buffer (50 mM) for maintaining a pH value similar to physiological conditions ($\text{pD} = 7.2$). The equilibrium state was reached in most of the cases within the first 10 min of reaction, in accordance with the fast rates of imine formation previously reported.⁴⁷ Notwithstanding, all reaction crudes were also monitored after 1, 24 and 48 h to assure that equilibrium was attained by noting only negligible changes in integration. Product abundances in Fig. 2 show interesting results in terms of structure-reactivity relationships. Salicylaldehyde (**A0**) did not react with **T** under the conditions assayed (Fig. 2). Aldehydes **A1** and **A3** resulted in conversions of *ca.* 60% into aldimine species, although the selectivity for the mono-over the bisimine product was quite low (75 and 83%, respectively, Fig. S1†). Compound **A2** showed a 16% yield for the monoimine derivative, but with excellent selectivity (Fig. 2 and S1†). Regarding pyridoxal derivatives, the aldehydes were nearly completely consumed after 1 h of reaction, indicating a clear electrophilic character for their carbonyl groups. Nevertheless, whereas **A4** tended to preferentially form the cyclic hemiacetal,

PLP (**A5**) led to *>90%* imine abundance. The enhanced activity of **A5** in comparison to **A1–3**, however, gave very low selectivity of monoimine species, as shown by the high abundance of the bisimine (**A5**)₂**T** (36%, Fig. 2). Regarding the aldehydes derived from **A6**, the nature of the sidechain was clearly affecting the imination outcome. Aldehyde **A6** was preferentially forming the hydrate derivative (60%), with only 9% of imine **A6T** being detected. When only one carboxylate anion was present in the structure (**A8** and **A9**), the aldimine yields were of *ca.* 10%, with excellent selectivities towards the monoimine derivatives. Satisfactorily, the reaction of **T** with **A7** (containing two anionic groups) led to good imine yields (48%, Fig. 2) with high selectivity for the mono-functionalized Schiff base (91%, Fig. S1†). As expected, increasing the equivalents of the triamino compound shifted the equilibrium towards the formation of the **A7T** monoimine product, with remarkable yield and selectivity (both values *>90%*, **A7*** in Fig. 2 and S1†). These preliminary results suggested that the imine stability was increased significantly by complementary electrostatic attractive forces between the

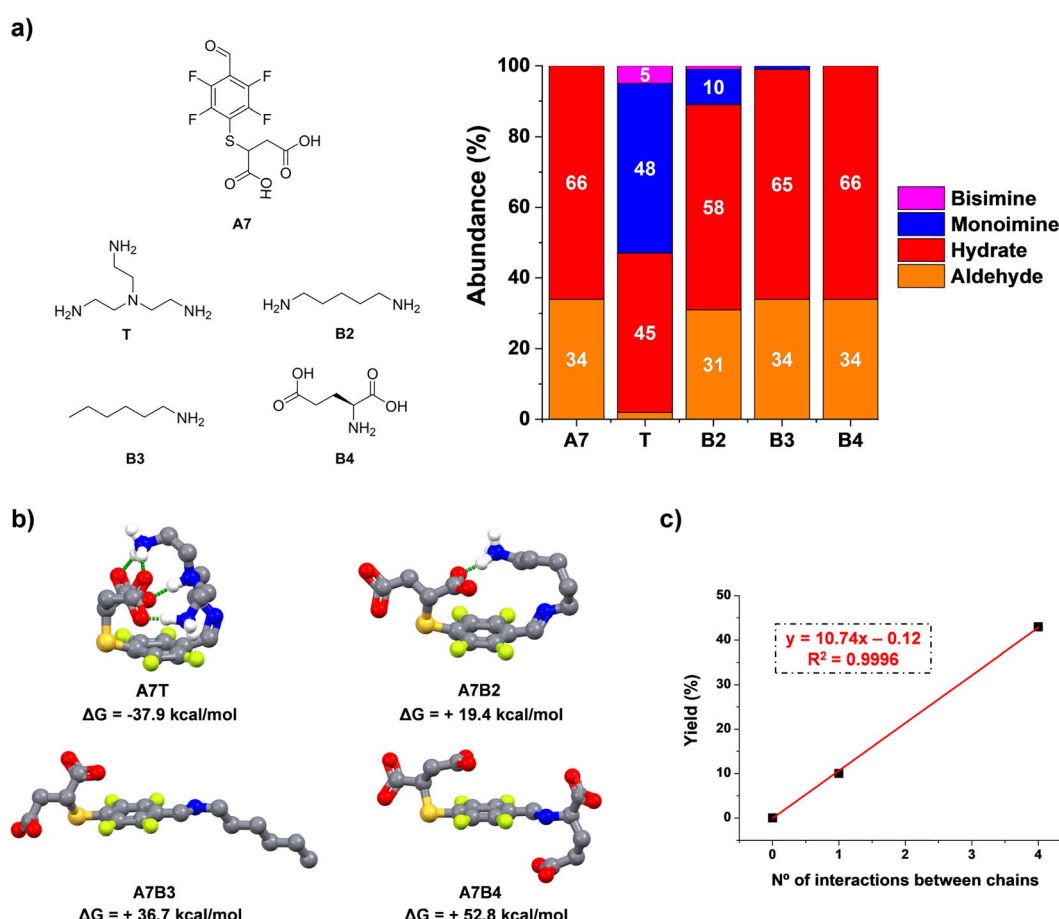


Fig. 3 (a) Chemical structures and component abundances (%) for reactions between aldehyde **A7** and model amines **T**/**B2–4**. Abundances calculated from ^1H NMR spectra (500 MHz, 295 K, D_2O). Reaction conditions: D_2O ($\text{pD} = 7.2$, phosphate buffer 50 mM), 295 K, 1 h, $[\text{A7}] = [\text{amine}] = 5 \text{ mM}$. The abundances of the bisimines were calculated considering the integration of two equivalent CHO protons. (b) DFT (b3lyp/6-31g(d,p); solvent = water) optimized geometries for the aldimine compounds. Free-energies of formation (kcal mol^{-1}) have been calculated using the free-energies of precursors and the water molecule released in each condensation. Hydrogen bonds/electrostatic forces between the two pendant arms of the building blocks have been highlighted with discontinuous green lines. Non-essential hydrogens have been omitted for clarity. (c) Linear fitting correlating the number of interactions between the sidechains and experimental yields attained in the imination reaction.

carboxylate and protonated amine groups of the multivalent sidechains, as well as by a contribution of the local concentration of reactive groups.

In the light of these results, we studied the condensation reaction between **A7** and model amino compounds containing different number of charges (**T** and **B2–4**, Fig. 3a). Thus, the reaction between **A7** and **B2** yielded a noticeable decrease in aldimine formation (43 vs. 10% for **A7T** and **A7B2**, respectively). In a similar manner, hexylamine (**B3**) gave only traces of imine under the same conditions (<1%, Fig. 3a). In this case there was no additional electrostatic interaction for promoting imine formation. As surmised, when **A7** was reacted with **B4** (each of them containing two negative charges on the residues) no imino-compound was detected even after 48 h of equilibration, likely due to the strong repulsion between the four negatively charged units. These results are in line with an increased stability of the imine species through supramolecular multivalency.

To corroborate the effect of secondary supramolecular interactions, DFT calculations were carried out for the different aldimine compounds, *viz.* **A7T**, **A7B2**, **A7B3**, and **A7B4**. As expected, all the optimized geometries adopted a *-trans* isomeric form for the imine bond. Regarding the non-covalent forces between chains, a significant energy difference was found for the extreme cases **A7T** and **A7B3/A7B4**. Whereas the most stable imine **A7T** adopts a tangled conformation assisted by four intramolecular polar hydrogen bonds, **A7B3** and **A7B4** rather adopted an expanded spatial distribution imposing large distances between the negatively charged chain of **A7** and the hydrophobic/anionic arm of **B3/B4** (Fig. 3b). An intermediate scenario was found for **A7B2**, forming only one intramolecular non-covalent interaction between units. In this case, the maximum yield of aldimine was of 10%, in agreement with the lower thermodynamic stability of this species in comparison with that presenting a higher degree of supramolecular multivalency (**A7T**). The plot for mono-imine yields *vs.* the number of non-covalent forces between chains revealed a linear trend (Fig. 3c). Therefore, these structural features appear desirable for the reversible bioconjugation of proteins containing a large number of positively charged residues (*e.g.*, Lys/Arg) that provide numerous supramolecular complementary forces with **A7**.

Reversible tethering of amino acids and small peptides: site-selective $\text{N}\alpha$ -functionalization

The next step towards the functionalization of proteins was to evaluate the reactivity of **A7** with different amino acid derivatives. The effect of the amino acid residue was studied by screening a set of five different canonical amino acids (Fig. 4a). The methyl ester derivatives (**XOMe**) were used in all cases to avoid repulsive electrostatic interactions between the corresponding carboxylate anions and those of **A7**. This aldehyde was able to form the desired imino species in 5–12% yields with the amino acid derivatives considered (Fig. 4b). The highest yield was attained for **ROME** (12%), likely as a result of the secondary electrostatic interactions between the charged guanidinium unit of **ROME** and the carboxylate groups of **A7**.

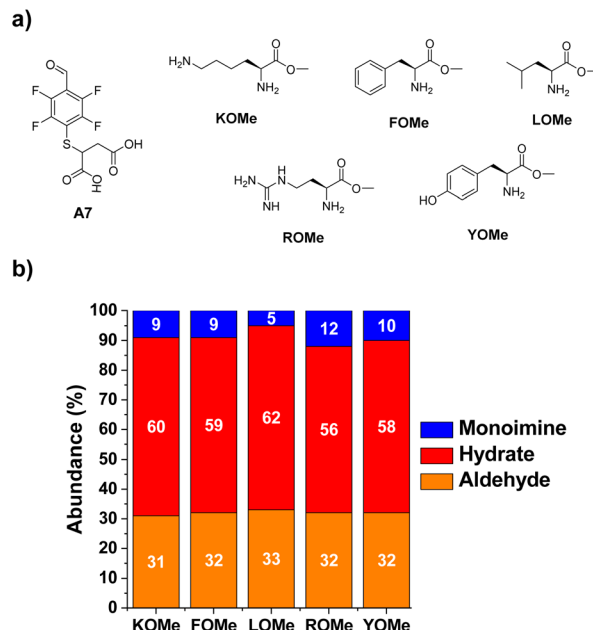


Fig. 4 (a) Chemical structures of the aldehyde **A7** and the different methyl ester derivatives of selected amino acids. (b) Component abundances (%) as calculated from ^1H NMR spectra (500 MHz, 295 K, D_2O). Reaction conditions: D_2O ($\text{pD} = 7.2$, phosphate buffer 50 mM), 295 K, 1 h, $[\text{A7}] = [\text{XOMe}] = 5 \text{ mM}$.

The reactions of **A7** with several Lys derivatives and small peptides were next examined as diverse recognition sites on the sidechains could provide additional driving forces (Fig. 5). The results agreed well with the proposed role of attractive and/or repulsive secondary electrostatic forces. The reaction between **A7** and **K** did not result in the formation of the corresponding **A7K**. Removing the negative charge of the carboxylate group in **K** by using its methyl ester derivative (**KOMe**) resulted in *ca.* 10% yield of **A7KOMe**, indicating that the carboxylate group in **K** was disfavoring the formation of the imine. Only one CH imine signal was detected in the ^1H NMR spectrum for the reaction between **A7** and **KOMe**, suggesting that the aldimine formation was regioselective. No imine was formed in the reaction between **A7** and $\text{AcN}\alpha\text{K}/\text{AcN}\alpha\text{KOMe}$. Hence, the reaction was clearly occurring at the $\text{N}\alpha$ site since when this position was blocked as an acetamide group, no aldimine was observed. This preferential reactivity of the $\text{N}\alpha$ is related to its lower basicity ($\text{pK}_a \approx 6\text{--}8$) compared to that of lysine ε -amino groups ($\text{pK}_a \approx 10$), as previously described.⁴⁶ Its lower basicity leads to a lower protonation of the terminal $-\text{NH}_2$, enhancing its propensity to act as a nucleophile and form the imine.

The bi- and tripeptidic Lys derivatives, namely **KK** and **KKK**, led only to a slight increase in the yields, 14 and 13% respectively. The selectivity for the $\text{N}\alpha$ -aldimine was excellent in all cases, with no additional imino compound detected in solution. As further validation of the reaction site specificity, 2D NMR analyses (HMBC and edited HSQC, Fig. S2†) revealed that the CH of the imine at 8.52 ppm was in close proximity to the chiral carbon of **A7KK** appearing at 73.7 ppm (Fig. S2b and c†). The most stable conformation calculated by DFT for **A7KK** inferred

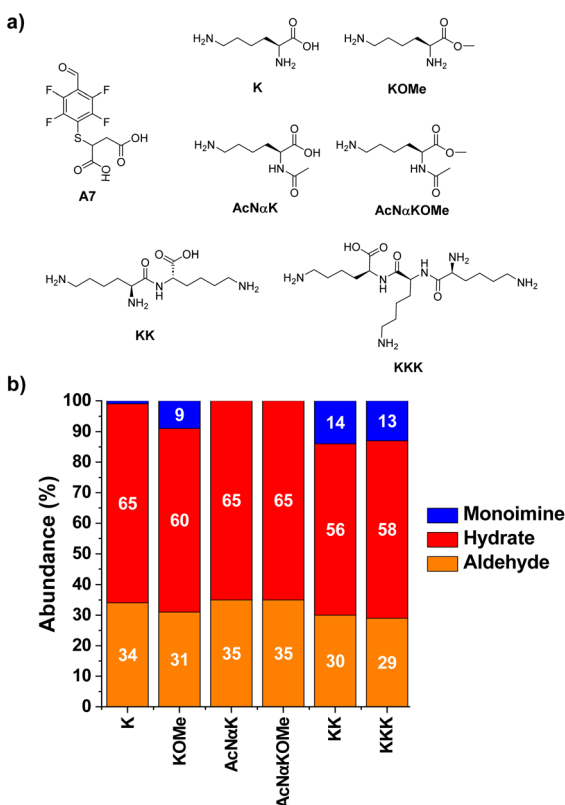


Fig. 5 (a) Chemical structures and (b) component abundances (%) as calculated from ^1H NMR (500 MHz, 295 K, D_2O) for the tested Lys derivatives upon reaction with A7. Reaction conditions: D_2O ($\text{pD} = 7.2$, phosphate buffer 50 mM), 295 K, 1 h, $[\text{A7}] = [\text{XKY}] = 5 \text{ mM}$.

the presence of only one attractive hydrogen bond/electrostatic interaction, involving one of the $\text{N}\varepsilon$ of KK and one of the carboxylate anions of the A7 chain (Fig. S3†). Therefore, the imine yield in the condensation between A7 and KK agrees well with that calculated using the linear correlation proposed in Fig. 3c (experimental: 14%; calculated: 11%). An increase in molar ratio KK/A7 up to 10 eq. of KK gave imine yields >40% and $\text{N}\varepsilon$ selectivities >99% (Fig. S4†). This remarkable selectivity may be of interest for the selective modification of the $-\text{NH}_2$ terminal of peptides and proteins.

As chirality may be expected to play a pivotal role in molecular recognition processes,^{48,49} the chiral aldehyde A8 was studied instead of the achiral A7. In all cases, the imine formation was lower than with A7, with the largest effect being observed for KOMe, in agreement with imine stabilization by attractive electrostatic interactions. In contrast, the affinity of A8 to form imines was significantly enhanced when using KK. The molar ratio effect on the final distribution of compounds was also studied once equilibrium was reached after 1 h of reaction. Comparing results obtained with those for A7, the cysteine-derived A8 gave higher imine yields (see for instance Fig. S4 and S6†), while maintaining excellent selectivities for the $\text{N}\varepsilon$ monoimine A8KK (>99%). When 10 eq. of KK were mixed with A8, A8KK was generated in an NMR yield of 62%. These results paved the way for exploring protein modifications using A7 and A8.

Bioorthogonal modification of carbonic anhydrase (CA) and dynamic regulation of its activity

Although a great number of important drugs exploit irreversible binding for inhibition, it has been considered that potential long-term toxicity has led to near exclusion from the discovery program.^{13,50} Moreover, the still critical challenge of site-selective protein bioconjugations emphasizes the need to develop novel strategies that can render bioorthogonal and regioselective conjugations.^{33,51} The use of reversible covalent ligation has offered advantages for dynamic protein tethering as dynamic bonds allow for the occurrence of error checking.^{52,53} Promising results in $\text{N}\varepsilon$ -selective modifications have recently taken advantage of its lower degree of protonation at physiological conditions.^{54–56} Aldimine formation has been proven useful for distinguishing between $\text{N}\varepsilon$ -sites of Lys residues, although a coupled irreversible nucleophilic attack was required for increasing the stability of conjugated units.^{33,34} In such examples, the microenvironment of each Lys residue was controlling their reactivity and, therefore, the regioselectivity outcome. This is of prior importance when discussing the so-called “hyper-reactive lysines” that present a markedly enhanced $\text{N}\varepsilon$ -nucleophilicity, presenting $\text{p}K_{\text{a}}$ values ≈ 5 units lower than solvent-exposed analogues.⁵⁷

As a consequence, we decided to explore whether the activity of a model enzyme, *i.e.* carbonic anhydrase (CA), could be dynamically modified by reaction with aldehydes A7/A8. CA is a ubiquitously found metalloenzyme playing an essential role in the preservation of acid–base homeostasis, pH regulation, and fluid balance, through the interconversion between CO_2 and bicarbonate ion.⁵⁸ In addition, its isomeric II form (hCAII) is found in many human tissues and is for instance responsible for maintaining inner eye pressure.⁵⁹ Therefore, many efforts have been devoted in the last years to designing adequate inhibitors for CA, as dysregulation of this enzyme is directly related to severe diseases like glaucoma.^{60,61} CA also presents esterase activity that facilitates the monitoring of its catalytic performance when interacting with different chemical species.⁶² CA from bovine erythrocytes was chosen for evaluating not only the efficiency of the bioconjugations but also their effect on its activity in the formation of *para*-nitrophenol from 4-nitrophenylacetate, **p-NP** and **p-NPA** respectively. One may note that the selection of CA as the model substrate took also into account the presence of 18 solvent-accessible Lys sites (marked in blue in Fig. 6a) that might facilitate the chemical modification with the proposed aldehydes.

UV monitoring of kinetic profiles for the hydrolysis of **p-NPA** catalyzed by 0.1 mol% of CA in the absence and presence of different amounts of A7 revealed a minor effect on its activity (Fig. 6b and c). For instance, introducing 100 equivalents of A7 (*i.e.*, 0.01 CA/A7 ratio) only led to a decrease in activity of *ca.* 15%. The addition of 1000 eq. of A7 was needed for reducing the catalytic activity of CA to $\approx 50\%$ of its initial value, suggesting that the bioconjugation of A7 was not critically altering the catalytic performance of the enzyme. In contrast, the treatment of CA with compound A8 promoted a strong inhibition of the biomolecule (Fig. 6d and S7†). The apparent half maximal

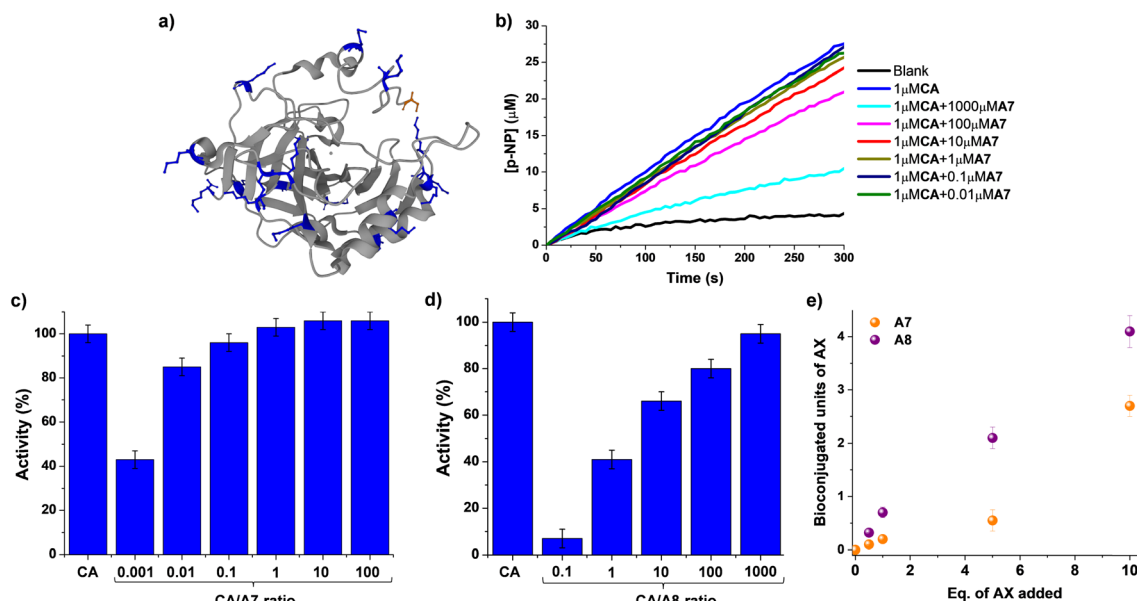


Fig. 6 (a) 3D-structure of native CA from bovine erythrocytes (pdb: 1v9e). The backbone of the protein (including α -helices and β -sheets) is colored grey. Lys (18 in total) and terminal $N\alpha$ sites (S1) are highlighted in blue and orange respectively, using the ball and stick model. (b) UV monitoring (linear range, 0–300 min) of the hydrolysis of *p*-NPA in the presence of CA and different equivalents of A7. Reaction conditions: D_2O ($pD = 7.2$), 335 K. Relative activities (%) observed for the different concentrations of A7 (c) and A8 (d) assayed. The activity of the native state CA (1 μM) has been used as reference. (e) Comparison of the MALDI analyses studying the CA bioconjugation efficiency in the presence of A7 and A8. The amount of units incorporated have been determined considering the increase in molecular weight of the CA, the equivalents of each aldehyde added, and the molecular weight of each aldehyde. See Fig. S8 \dagger for fitted curves, and S30–40 \dagger for full m/z scale MALDI analyses. MALDI conditions: PNA matrix, D_2O , $pD = 7.2$, phosphate buffer. CA concentration = 0.1 mM. Error bars calculated considering the width of the Gaussian distribution for each sample.

inhibitory concentration (IC_{50}) value was of *ca.* 1 μM , corresponding to a 1 : 1 molar ratio with CA. In the presence of 10 equivalents of A8, the activity of the enzyme was reduced to 7% of its initial value, stressing the inhibiting potential of A8.

MALDI analyses showed an increase in the molecular weight of the biomolecule dependent on the equivalents of AX introduced (Fig. S8 \dagger). These results indicate a much stronger effect of A8 than of A7 (Fig. 6e). When 1 eq. of A8 was added to the protein, an increase in molecular weight of *ca.* 300 g mol $^{-1}$ was noted, in accordance with the tethering of 0.7 units of A8. 63 On the other hand, the introduction of 1 eq. of A7 led to the incorporation of only 0.2 units of A7. Similarly, the use of 5 eq. of the aldehydes resulted in the binding of 2 and 0.5 units for A8 and A7, respectively. At higher excesses of aldehydes (*i.e.*, 10 eq.) 3 and 4 units of A7 and A8 were respectively bound to CA. Neither the CA molecular weight nor its enzymatic activity were altered in the presence of 10 eq. of A0 (Fig. S9 \dagger). Therefore, the supramolecular multivalency effects are crucial for the CA dynamic tethering and regulation of its activity. These outcomes point to promising applications of DCC in site-selective bioconjugations since, despite the high frequency of Lys sites in CA, only the thermodynamically favored sites were effectively functionalized even when adding an excess of the reactive species.

The tethering of A8 to CA was studied in greater detail to shed light on the nature of its inhibitory activity. 1H NMR titration experiments suggested the appearance of a low-intensity peak at 8.43 ppm, assigned to the formation of

aldimine derivatives with the protein (Fig. S10a \dagger). The presence of the CHO signal (9.97 ppm) even at <5 eq. of A8 supports the incomplete bioconjugation (only thermodynamically favored sites), observed in the MALDI analyses. Interestingly, some regions of the protein seemed to experience a noticeable change in the electronic environment as a result of the dynamic modification (Fig. S10b \dagger). Circular dichroism (CD) titration experiments showed a similar scenario, with CA undergoing a conformational modification in the presence of A8 (Fig. S11 and S12 \dagger). The negative band centered at 219 nm, ascribed to β -sheet-like arrangements in the native state of the protein, seemed to decrease in intensity with increasing amounts of A8, suggesting that some sections of the β -sheets were being perturbed. Considering the structural features of A8, one might surmise that the inhibition mode of action can rely on allosteric processes, in which the conformational changes induced by aldimine modifications reduced the efficiency of the catalyst. The 3D structure of native CA shows a highly hindered active site located in the center of a conical cavity defined by curved β -sheets (see Fig. S13a \dagger). 64 The most plausible trajectory for *p*-NPA to reach the active site is its diffusion through the conical cavity, in the entrance of which are located a terminal Ser (S1) group and a Lys residue (K168) (see spacefilling residues in Fig. S13a \dagger). Preliminary docking experiments were carried out for studying the preferential recognition sites for A8 in the CA structure, using SwissDock. 65 A blind and accurate docking was selected for screening all possible recognition sites. The top-ranked position (binding free-energy: -8.15 kcal mol $^{-1}$)

located **A8** near the terminal $\text{N}\alpha$ unit and K168 , stabilized through several non-covalent forces with peptidic bonds and amino acid residues (Fig. S13b and c†). For instance, the carboxylate group of **A8** is tightly bound to **S1** through two hydrogen bonds, one with its terminal amino group and one with the NH of the S1-H2 peptidic bond, with distances between heavy atoms of 2.753 and 2.517 Å, respectively. The negatively charged unit of E234 seems to be interacting by means of anion- π forces ($\text{O}_{\text{E234}} \cdots \text{C}_{\text{ar},\text{A8}} = 3.059$ Å) with the electron-deficient tetrafluoro-substituted aromatic ring of **A8**. Additional $\text{CH} \cdots \pi$ interactions between the Cbz -aromatic motif of **A8** and the imidazole ring of **H3** could be further stabilizing the host-guest adduct ($\text{CH}_{\text{H3}} \cdots \text{C}_{\text{ar},\text{A8}} = 2.674$ Å). The formation of the aldimine derivative is likely to occur in that specific pocket as a result of the increased local concentration of the nucleophilic scaffolds ($\text{N}\varepsilon\text{-Lys168}/\text{N}\alpha\text{-Ser1}$) and the electrophilic CHO group of **A8**. Hence, the imine formation between **CA** and **A8** might hamper the diffusion of *p*-NPA to the active site, leading to allosteric regulation of the enzymatic activity.⁶⁶

Since the bioconjugations were based on imine formation, we considered that the reversible covalent bonds could be displaced by the influence of an external molecule, offering a mechanism to revert the modification of **CA** by **A8**. One may presume that the introduction of an acylhydrazide can trigger a release of the dynamic residue through aldimine component

exchange, as acylhydrazones present a higher thermodynamic stability than imines.⁴⁷ Girard's reagent **T** (**H1**, Fig. 7b) was selected as the potential effector as it contains a positively charged moiety in its structure, which might favor the rearrangement process through attractive supramolecular interactions with the carboxylate group of **A8**. The kinetic profile for the formation of **A8H1** from **A8** and **H1** was studied using ^1H NMR spectroscopy (Fig. S14†). After 2 h of reaction, poor yields were obtained when the two reagents were mixed in a 1:1 molar ratio. On the other hand, the addition of 10 eq. of **H1** led to yields higher than 50% in 30 min of reaction, with almost quantitative formation of the aldimine after 120 min (Fig. S14†). MALDI analysis of a sample containing **CA**, 10 eq. of **A8**, and 50 eq. of **H1** showed a decrease in m/z in comparison with the value measured for the inhibited enzyme (see green and purple distributions in Fig. 7a, respectively). Therefore, acylhydrazide **H1** seemed to be able to react with the bioconjugated units of **A8** to form **A8H1**, releasing **CA** in its native state. This was in good accordance with the catalytic assays performed. Upon introduction of **H1** (10 μM) in a solution containing the inhibited enzyme (1 μM **CA** + 1 μM **A8**), and equilibration for 2 h to assure the complete formation of acylhydrazone, the initial rates of *p*-NPA hydrolysis provided by native **CA** were attained (Fig. 7b). These results highlight the potential of using dynamic inhibitors based on reversible covalent bonds that permit an “on-off”

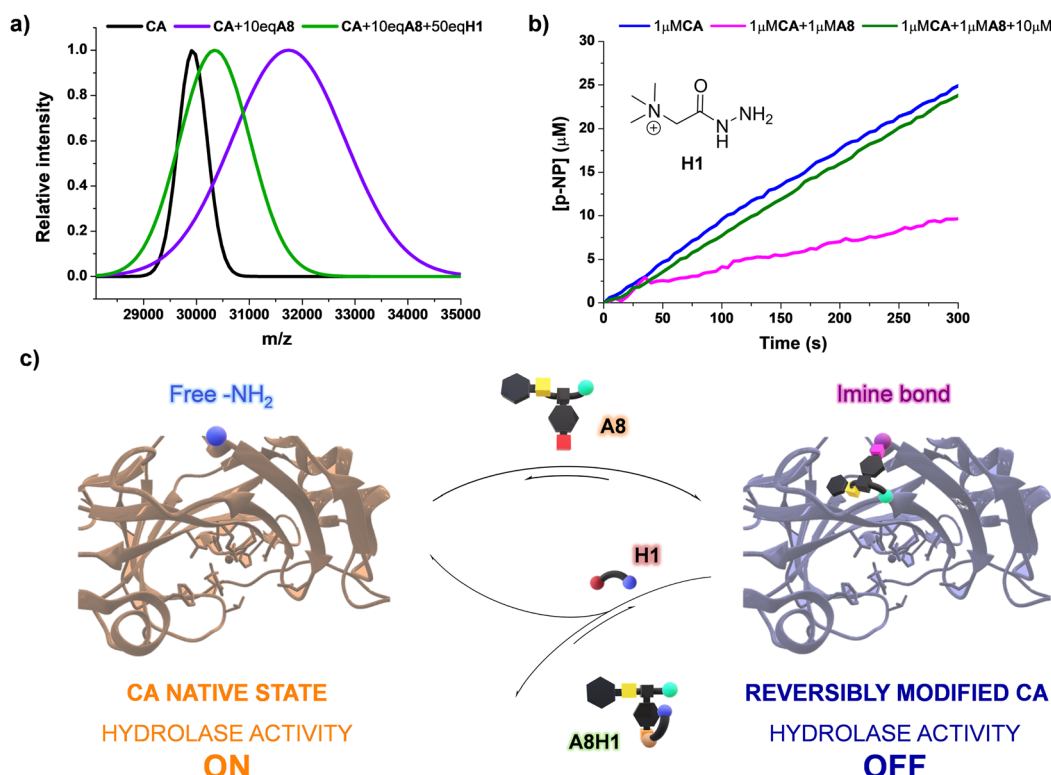


Fig. 7 (a) MALDI analyses (PNA matrix, D_2O , pH 7.2 phosphate buffer) for the bioconjugated (**A8**)₂**CA** (0.1 mM) in the presence and absence of effector **H1**. The peaks were fitted to a Gaussian distribution. The dispersity of the bioconjugation was estimated using the standard deviation of the fitting: **CA** ($\sigma = 271.9$), **CA** + 10 eq. **A8** ($\sigma = 1104.1$), **CA** + 10 eq. **A8** + 50 eq. **H1** ($\sigma = 665.6$). See Fig. S30–40† for full m/z scale MALDI analyses. (b) UV monitoring (linear range, 0–300 min) of the adaptive regulation proposed for the hydrolysis of *p*-NPA in the presence of **CA**, **A8**, and **H1**. Reaction conditions: D_2O (pH = 7.2), 335 K. See Fig. S15† for the kinetic profile obtained in the presence of solely **CA** (1 μM) and **H1** (10 μM). (c) Representation of the “turn on-off” hydrolase activity of *p*-NPA attained using **A8** and **H1** as dynamic effectors.

bioconjugations to control sophisticated enzymatic processes (Fig. 7c).

Conclusions and perspectives

Herein we showed that by exploiting supramolecular multivalent complementarity, one can efficiently drive imine formation even under physiological conditions. Specifically, combined electrostatic forces and hydrogen bonds between sidechains of amines and aldehydes can enhance the stability of the corresponding imines. This approach was further corroborated by simple experiments using model substrates, showing that in the cases where a supramolecular mismatch was introduced (e.g., two building blocks containing negatively charged units), no aldimine product was observed. The best-performing aldehydes **A7** and **A8** among those studied here, were reacted with amino acid derivatives and small peptides, yielding excellent selectivities for the functionalization of the terminal $\text{N}\alpha$, even in substrates containing competing sites. The bioconjugation to carbonic anhydrase (**CA**) was also assayed for studying the aldimine formation in biomolecules with such high functional density, observing that up to four units of **A8** were apparently bound to **CA** using 10 eq. of aldehyde. Spectroscopic analyses revealed that these modifications based on reversible covalent bonds were perturbing the 3D-structure of the protein, opening the way to studying their effect on the enzymatic activity. Remarkably, although **A7** barely affected the catalytic performance of **CA**, the introduction of 10 eq. of **A8** resulted in 93% inhibition of the initial enzymatic activity. Moreover, thanks to the reversible nature of the imine bonds, it was possible to design a “turn on-off” process in which the introduction of an effector, namely **H1**, led to the recovery of the native activity of **CA**. Such adaptive modifications of proteins showcase the enzymatically-reversible transformations that maintain the metabolic balance as a function of molecular environmental requirements. The implementation of the concept of supramolecular multivalency may become a major asset for improving the efficiencies of challenging reactions in highly competitive media.

Data availability

The ESI† contains experimental details, characterization, spectral data, computational data and cartesian coordinates.

Author contributions

The manuscript was written through contributions of all authors. All authors have given approval to the final version of the manuscript. Conceptualization: F. E., J. M. L. Data curation: F. E., F. R., formal analysis: F. E. Funding acquisition: J. M. L. Investigation: F. R. (supporting), F. E. (lead). Methodology: F. E. Project administration: J. M. L. Resources: J. M. L. Supervision: F. E., J. M. L. Validation: F. E. Visualization: F. R. (supporting), F. E. (lead), writing original draft: F. E. Writing – review and editing: F. R. (supporting), F. E., J. M. L.

Conflicts of interest

There are no conflicts to declare.

Acknowledgements

This work was supported by the ERC (Advanced Research Grant SUPRADAPT 290585), the University of Strasbourg Institute for Advanced Study (USIAS), and Fondation Jean-Marie Lehn. F. E. acknowledges Fundación Ramón Areces for a postdoctoral fellowship. The authors thank Dr J. L. Schmitt, Dr A. Osypenko, Dr Z. Yang, Dr S. Jung, T. Rieu, B. Kozibroda, M. J. Aguilera, and C. Antheaume for helpful discussions.

References

- 1 J. Wang, X. Wang, X. Fan and P. R. Chen, *ACS Cent. Sci.*, 2021, **7**, 929–943.
- 2 J. T. George and S. G. Srivatsan, *Chem. Commun.*, 2020, **56**, 12307–12318.
- 3 E. M. Sletten and C. R. Bertozzi, *Angew. Chem., Int. Ed.*, 2009, **48**, 6974–6998.
- 4 J. M. Lehn, *Angew. Chem., Int. Ed.*, 2015, **54**, 3276–3289.
- 5 J. M. Lehn, *Chem. Soc. Rev.*, 2007, **36**, 151–160.
- 6 Q. Laurent, R. Martinent, B. Lim, A.-T. Pham, T. Kato, J. López-Andarias, N. Sakai and S. Matile, *JACS Au*, 2021, **1**, 710–728.
- 7 Y. Zhang, Y. Qi, S. Ulrich, M. Barboiu and O. Ramström, *Mater. Chem. Front.*, 2020, **4**, 489–506.
- 8 Y. Jin, C. Yu, R. J. Denman and W. Zhang, *Chem. Soc. Rev.*, 2013, **42**, 6634–6654.
- 9 E. Raczkuk, B. Dmochowska, J. Samaszko-Fiertek and J. Madaj, *Molecules*, 2022, **27**, 787.
- 10 D. L. Wilson and E. T. Kool, Ultrafast Oxime Formation Enables Efficient Fluorescence Light-up Measurement of DNA Base Excision, *J. Am. Chem. Soc.*, 2019, **141**, 19379–19388.
- 11 X. Wang, Z. Lin, K. A. Bustin, N. R. McKnight, W. H. Parsons and M. L. Matthews, *J. Am. Chem. Soc.*, 2022, **144**, 5377–5388.
- 12 R. M. Reja, W. Wang, Y. Lyu, F. Haeffner and J. Gao, *J. Am. Chem. Soc.*, 2022, **144**, 1152–1157.
- 13 J. Pettinger, K. Jones and M. D. Cheeseman, *Angew. Chem., Int. Ed.*, 2017, **56**, 15200–15209.
- 14 J. I. Macdonald, H. K. Munch, T. Moore and M. B. Francis, *Nat. Chem. Biol.*, 2015, **11**, 326–331.
- 15 P. M. S. D. Cal, J. B. Vicente, E. Pires, A. V. Coelho, L. F. Veiros, C. Cordeiro and P. M. P. Gois, *J. Am. Chem. Soc.*, 2012, **134**, 10299–10305.
- 16 C. Givelet, J. Sun, D. Xu, T. J. Emge, A. Dhokte and R. Warmuth, *Chem. Commun.*, 2011, **47**, 4511–4513.
- 17 C. Godoy-Alcántar, A. K. Yatsimirsky and J. M. Lehn, *J. Phys. Org. Chem.*, 2005, **18**, 979–985.
- 18 R. B. Silverman, *Chem. Rev.*, 2018, **118**, 4037–4070.
- 19 A. Amadasi, M. Bertoldi, R. Contestabile, S. Bettati, B. Cellini, M. Luigi Di Salvo, C. Borri-Voltattorni, F. Bossa and A. Mozzarelli, *Curr. Med. Chem.*, 2007, **14**, 1291–1324.
- 20 F. B. L. Cougnon, K. Caprice, M. Pupier, A. Bauzá and A. Frontera, *J. Am. Chem. Soc.*, 2018, **140**, 12442–12450.



21 K. Caprice, M. Pupier, A. Kruve, C. A. Schalley and F. B. L. Cougnon, *Chem. Sci.*, 2018, **9**, 1317–1322.

22 R. Breslow, *Acc. Chem. Res.*, 1991, **24**, 159–164.

23 M. S. Li, Y. W. Dong, M. Quan and W. Jiang, *Angew. Chem., Int. Ed.*, 2022, **61**, e202208508.

24 E. Lutz, E. Moulin, V. Tchakalova, D. Benczédi, A. Herrmann and N. Giuseppone, *Chem. – Eur. J.*, 2021, **27**, 13457–13467.

25 K. Meguellati, A. Fallah-Araghi, J. C. Baret, A. el Harrak, T. Mangeat, C. M. Marques, A. D. Griffiths and S. Ladame, *Chem. Commun.*, 2013, **49**, 11332–11334.

26 Y. Lei, Z. Li, G. Wu, L. Zhang, L. Tong, T. Tong, Q. Chen, L. Wang, C. Ge, Y. Wei, Y. Pan, A. C. H. Sue, L. Wang, F. Huang and H. Li, *Nat. Commun.*, 2022, **13**, 3557.

27 Y. Lei, Q. Chen, P. Liu, L. Wang, H. Wang, B. Li, X. Lu, Z. Chen, Y. Pan, F. Huang and H. Li, *Angew. Chem., Int. Ed.*, 2021, **60**, 4705–4711.

28 Y. Chen, G. Wu, B. Chen, H. Qu, T. Jiao, Y. Li, C. Ge, C. Zhang, L. Liang, X. Zeng, X. Cao, Q. Wang and H. Li, *Angew. Chem., Int. Ed.*, 2021, **60**, 18815–18820.

29 Y. Chen, Y. Lei, L. Tong and H. Li, *Chem. – Eur. J.*, 2022, **28**, e202102910.

30 Z. She, H. Zou and L. You, *Org. Biomol. Chem.*, 2022, **20**, 6897–6904.

31 V. Saggiomo and U. Lüning, *Eur. J. Org. Chem.*, 2008, **25**, 4329–4333.

32 D. Carbajo, Y. Pérez, M. Guerra-Rebollo, E. Prats, J. Bujons and I. Alfonso, *J. Med. Chem.*, 2022, **65**, 4865–4877.

33 T. Sahu, M. Chilamari and V. Rai, *Chem. Commun.*, 2022, **58**, 1768–1771.

34 M. Chilamari, N. Kalra, S. Shukla and V. Rai, *Chem. Commun.*, 2018, **54**, 7302–7305.

35 L. Purushottam, S. R. Adusumalli, U. Singh, V. B. Unnikrishnan, D. G. Rawale, M. Gujrati, R. K. Mishra and V. Rai, *Nat. Commun.*, 2019, **10**, 2539.

36 L. Purushottam, S. R. Adusumalli, M. Chilamari and V. Rai, *Chem. Commun.*, 2017, **53**, 959–962.

37 E. F. Oliveira, N. M. F. S. A. Cerqueira, P. A. Fernandes and M. J. Ramos, *J. Am. Chem. Soc.*, 2011, **133**, 15496–15505.

38 M. Bru, I. Alfonso, M. Bolte, M. I. Burguete and S. V. Luis, *Chem. Commun.*, 2011, **47**, 283–285.

39 I. Casciuc, A. Osypenko, B. Kozibroda, D. Horvath, G. Marcou, F. Bonachera, A. Varnek and J. M. Lehn, *ACS Cent. Sci.*, 2022, **8**, 804–813.

40 J. D. Badjic, A. Nelson, S. J. Cantrill, W. B. Turnbull and J. F. Stoddart, *Acc. Chem. Res.*, 2005, **38**, 723–732.

41 J. D. Badjic, S. J. Cantrill, R. H. Grubbs, E. N. Guidry, R. Orenes and J. F. Stoddart, *Angew. Chem., Int. Ed.*, 2004, **43**, 3272–3278.

42 Y. Zhuo, X. Wang, S. Chen, H. Chen, J. Ouyang, L. Yang, X. Wang, L. You, M. Utz, Z. Tian and X. Cao, *Chem. – Eur. J.*, 2021, **27**, 9508–9513.

43 L. S. Witus, C. Netirojjanakul, K. S. Palla, E. M. Muehl, C. H. Weng, A. T. Iavarone and M. B. Francis, *J. Am. Chem. Soc.*, 2013, **135**, 17223–17229.

44 F. Thaler, C. D. Hubbard, F. W. Heinemann, R. van Eldik, S. Schindler, I. Fábián, A. M. Dittler-Klingemann, F. E. Hahn and C. Orvig, *Inorg. Chem.*, 1998, **37**, 4022–4029.

45 G. Anderegg and V. Gramlich, *Helv. Chim. Acta*, 1994, **77**, 685–690.

46 C. Sornay, V. Vaur, A. Wagner and G. Chaubet, *R. Soc. Open Sci.*, 2022, **9**, 211563.

47 M. He and J. M. Lehn, *J. Am. Chem. Soc.*, 2019, **141**, 18560–18569.

48 P. Peluso and B. Chankvetadze, *Chem. Rev.*, 2022, **122**, 13235–13400.

49 X. Zhang, J. Yin and J. Yoon, *Chem. Rev.*, 2014, **114**, 4918–4959.

50 C. González-Bello, *ChemMedChem*, 2016, **11**, 22–30.

51 J. M. Gilmore, R. A. Scheck, A. P. Esser-Kahn, N. S. Joshi and M. B. Francis, *Angew. Chem., Int. Ed.*, 2006, **45**, 5307–5311.

52 A. Bandyopadhyay and J. Gao, *Curr. Opin. Chem. Biol.*, 2016, **34**, 110–116.

53 G. Akçay, M. A. Belmonte, B. Aquila, C. Chuaqui, A. W. Hird, M. L. Lamb, P. B. Rawlins, N. Su, S. Tentarelli, N. P. Grimster and Q. Su, *Nat. Chem. Biol.*, 2016, **12**, 931–936.

54 H. Jiang, W. Chen, J. Wang and R. Zhang, *Chin. Chem. Lett.*, 2022, **33**, 80–88.

55 S. Wang, Q. Zhou, X. Chen, R. H. Luo, Y. Li, X. Liu, L. M. Yang, Y. T. Zheng and P. Wang, *Nat. Commun.*, 2021, **12**, 2257.

56 J. R. Deng, N. C. H. Lai, K. K. Y. Kung, B. Yang, S. F. Chung, A. S. L. Leung, M. C. Choi, Y. C. Leung and M. K. Wong, *Commun. Chem.*, 2020, **3**, 67.

57 S. M. Hacker, K. M. Backus, M. R. Lazear, S. Forli, B. E. Correia and B. F. Cravatt, *Nat. Chem.*, 2017, **9**, 1181–1190.

58 C. T. Supuran, *Nat. Rev. Drug Discovery*, 2008, **7**, 168–181.

59 V. M. Krishnamurthy, G. K. Kaufman, A. R. Urbach, I. Gitlin, K. L. Gudiksen, D. B. Weibel and G. M. Whitesides, *Chem. Rev.*, 2008, **108**, 946–1051.

60 I. Huc and J. M. Lehn, *Proc. Natl. Acad. Sci. U.S.A.*, 1997, **94**, 2106–2110.

61 S. Kumar, S. Rulhania, S. Jaswal and V. Monga, *Eur. J. Med. Chem.*, 2021, **209**, 112923.

62 J. D. Cheeseman, A. D. Corbett, R. Shu, J. Croteau, J. L. Gleason and R. J. Kazlauskas, *J. Am. Chem. Soc.*, 2002, **124**, 5692–5701.

63 Note: units calculated taking into account the added equivalents of **AX** (theoretical value), the increase in molecular weight observed in the MALDI spectrum (**CA** + **AX**), and the molecular weight of each aldehyde. The results showing conjugation units smaller than 1 are assigned to the overlayed distribution of conjugated and non-conjugated species. See Fig. 6e for details.

64 E. Marcos, B. Basanta, T. M. Chidyausiku, Y. Tang, G. Oberdorfer, G. Liu, G. V. T. Swapna, R. Guan, D.-A. Silva, J. Dou, J. H. Pereira, R. Xiao, B. Sankaran, P. H. Zwart, G. T. Montelione and D. Baker, *Science*, 2017, **355**, 201–206.

65 A. Grosdidier, V. Zoete and O. Michielin, *Nucleic Acids Res.*, 2011, **39**, W270–W277.

66 N. V. Dokholyan, *Chem. Rev.*, 2016, **116**, 6463–6487.

